Supporting Information

Electrochemical Reduction of Functionalized Carbonyl Compounds: Enhanced Reactivity over Tailored Nanoporous Gold

Zihui Xiao, Hui Yang, Shuai Yin, Jian Zhang, Zhenhua Yang, Kedong Yuan,* and Yi Ding*

Tianjin Key Laboratory of Advanced Functional Porous Materials, Institute for New Energy Materials and Low-Carbon Technologies, School of Materials Science and Engineering, Tianjin University of Technology, Tianjin 300384, China.

* E-mail: yding@tjut.edu.cn; kedong.yuan@tjut.edu.cn.

Experimental information

Reagents and electrodes

Commercial reagents, such as *p*-nitrobenzaldehyde (*p*-NBD), diphenylsilane, tetrabutylammonium tetrafluoborate (Bu_4NBF_4), CH_3CN (HPLC grade) and H_2SO_4, were used as received without further purification. The electrode materials, including bulk Zn, Fe, Al, Pb, Pt, Cu, Ag, Au, AuAg alloy, glassy carbon and graphite, were obtained from IKA WORKS GUANGZHOU.

Preparation of NPG electrode

NPG films with different pore size were obtained by dealloying $Au_{50}Ag_{50}$ (at.%) foils via free etching. Specifically, the $Au_{50}Ag_{50}$ foils were floated upon 67 wt% HNO_3 at 5 °C for 30 min, 20 °C for 30 min and 30 °C for 120 min, respectively. The corresponding NPG films with pore size of 15, 30 and 50 nm could be obtained, which were defined as NPG-S, NPG-M and NPG-L. The obtained NPG films were washed 3-4 times with ultrapure water and finally adhered to the glassy carbon electrode with polyvinylidene fluoride as agglomerant.

The NPG-M@Au and NPG-M@Ag were obtained by electrochemical reduction method, where the NPG-M was coated with Au (Ag) in a N_2-saturated mixture solution of 0.1 M $HClO_4$ and 0.5 mM $HAuCl_4$ ($AgNO_3$) at 0.8 V (0.1V) versus SCE for 10 min.

Structural characterization

Powder X-ray diffraction (XRD) data were measured on a SmartLab 9KW diffractometer with a Cu Kα monochromatized radiation source (λ=1.5418 Å), operated at 40 KV and 30 mA.

The morphology of samples was observed by scanning electron microscopy (SEM, FEI Verios 460L) and a high-resolution transmission electron microscope (TEM, FEI Talos F200X) (operated at 200 kV).

X-ray photoelectron spectroscopy (XPS) measurements were carried out on a ThermoFisher ESCALAB 250Xi. Monochromatic Al Kα (1486.6 eV) x-ray source was used as incident radiation. The base pressure in the measurement chamber was 2 x 10^{-10} mbar. The analyzer slit was set to 0.4

mm and a pass energy of 200 eV was chosen, resulting in an overall energy resolution better than 0.5 eV. Charging effects were compensated by use of a flood gun. The binding energies were calibrated using the C1s peak at 285 eV as a reference. The XPS peaks are analyzed using a Shirley-type background and a nonlinear least-squares fitting of the experimental data based on a mixed Gaussian/Lorentzian peak shape.

Electrochemical characterization

A CHI760E electrochemical workstation (CH Instrument Inc. USA) was employed to carry out Linear Sweep Voltammetry (LSV) and Cyclic Voltammetry (CV) utilizing a three-electrode cell system. Electrochemical Impedance Spectroscopic (EIS) measurements were also performed, where the frequency was varied from 0.1 Hz to 1×10^5 Hz with an A.C. voltage amplitude of 10 mV. An Ag/AgCl (3.0 M KCl) and a graphite plate were used as the reference electrode and the counter electrode, respectively. The reaction kinetics of *p*-nitrobenzaldehyde reduction at the different NPG electrodes was analyzed using the Tafel plot.

Electrochemically active surface area (ECSA) measurement: To determine the ECSA, CV measurements were performed at room temperature in an N_2-purged 0.5 M H_2SO_4 with a scan rate of 50 mV s^{-1} and a potential range between -0.24 V to 1.46 V (vs. Ag/AgCl), which can provide direct chemical identification of species exposed to the electrolyte. And a graphite plate and Ag/AgCl (3 M KCl) were used as the counter electrode and the reference electrode, respectively. Before CV measurement, the working electrode was pretreated electrochemically for 10 cycles until a stable CV curve was obtained. The EASA was determined by integrating the reduction peak (centered at ~0.9 V vs. Ag/AgCl) to calculate the charge that was associated with the reduction peak.

Electrochemical Measurements

All measurements were carried out in a H-type cell (10 mL per chamber) with cation exchange membrane (DuPont® Nafion-117). Pretreatment of the electrodes was carried out to remove the metal oxides, which can deactivate the reaction when existing on the electrode surface. After polishing with sand paper, Zn, Fe, Al, Pb, Pt, Cu, Ag, Au, AuAg alloy electrodes were acid washed with 1 M HCl solution for 0.5 h. After pretreatment, all electrodes were rinsed with deionized water.

The current density (mA cm^{-2}) was obtained based on geometric area (1.2 cm^2). In all experiments, an Ag/AgCl (3.0 M KCl) and a graphite plate were used as the reference electrode and the counter electrode**.**

Product analysis

The products were filtered through a short silica gel column to remove the electrolyte, and a small partial of solution was analysed with a PerkinElmer Clarus 580 gas chromatograph equipped with a flame ionization detector (Elite-5 GC column: 30 m×0.25 mm×0.25 μm), where *n*-decane as internal standard. The TOF value was calculated based on the ECSA as following:

$$\mathrm{TOF} = \frac{mol\ of\ p-NBD\ converted}{mol\ of\ surface\ Au\ atoms \times reaction\ time\ (h)}$$

$$\text{Mol of surface Au atoms} = \frac{ECSA \times 10^{16}}{2\pi R^2 \times NA}$$

Wherein, R is the radius of Au atom (1.79 Å); NA is Avogadro's constant (6.02×10^{23}).

General procedure for electrochemical reduction of carbonyl compounds

As a typical experiment, a H-type cell (10 mL per chamber，divided by a cation exchange membrane, DuPont® Nafion-117) was charged with an NPG-M (1.2 cm^{-2}) film as a working electrode, an Ag/AgCl (3.0 M KCl) as the reference electrode and a graphite plate as the counter electrode, which were connected to an electrochemical workstation regulated power supply. To this cell, Bu_4NBF_4 (0.20 mmol, 65.9 mg), CH_3CN (10 mL) were added to each chamber, and Ph_2SiH_2 (1.0 mmol, 184.3 mg), *p*-nitrobenzaldehyde (1.0 mmol, 151.1 mg) were added in the cathodic chamber. Then the reaction mixture was electrolyzed under -0.6 V constant potential at room temperature with magnetic stirring until *p*-nitrobenzaldehyde was completely converted (monitored by TLC). After the reaction, dodecane (50 μL) was added to the solution as an internal standard for GC analysis. Known products were further analyzed by using GC-MS, ^{1}H NMR and verified by comparison of authentic samples.

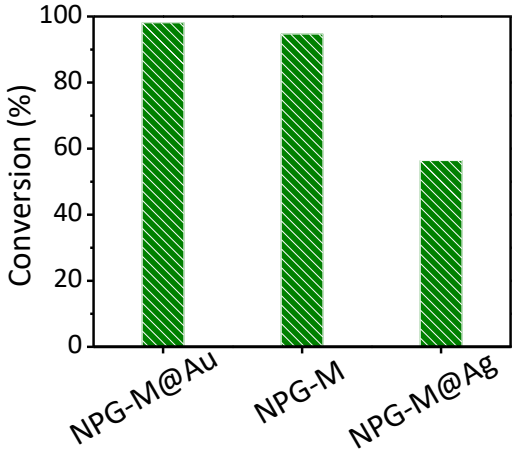

Fig. S1 Influence of Ag on the catalytic performance.

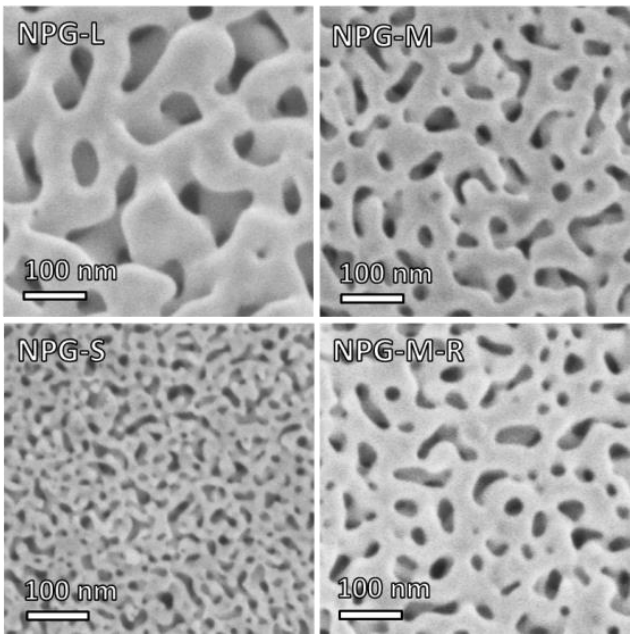

Fig. S2 SEM images of the NPG catalysts before and after reaction.

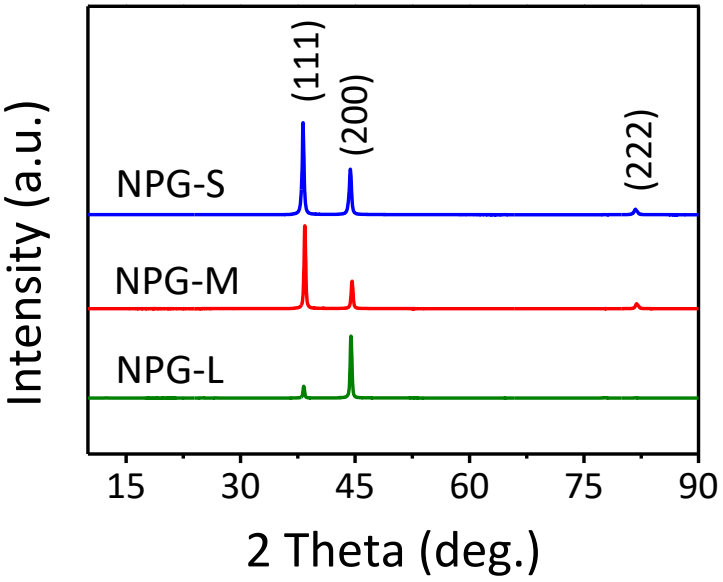

Fig. S3 XRD patterns of the NPG catalysts.

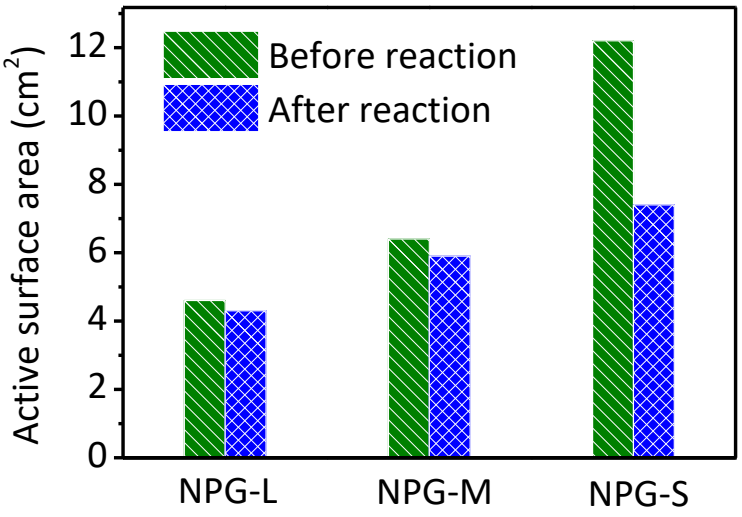

Fig. S4 Active surface area of the NPG catalysts before and after reaction.

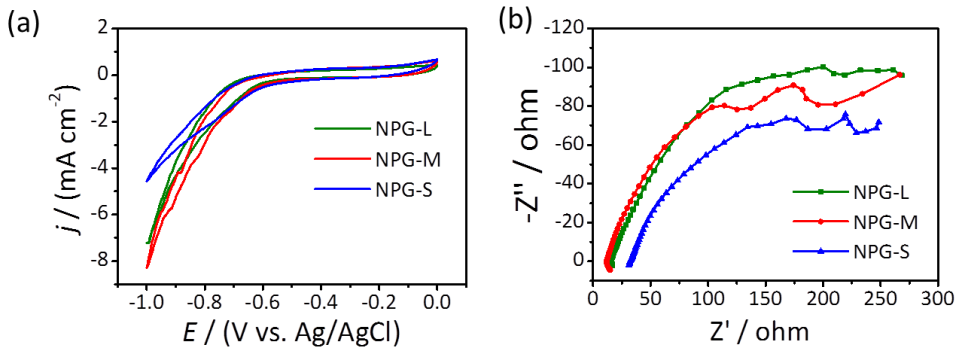

Fig. S5 CV curves of the NPG electrodes in CH_3CN with substrates (a); Nyquist plots measured at −0.6 V (vs. Ag/AgCl) in CH_3CN with substrates (b). Substrates: 1 mmol *p*-NBD, 1 mmol Ph_2SiH_2.

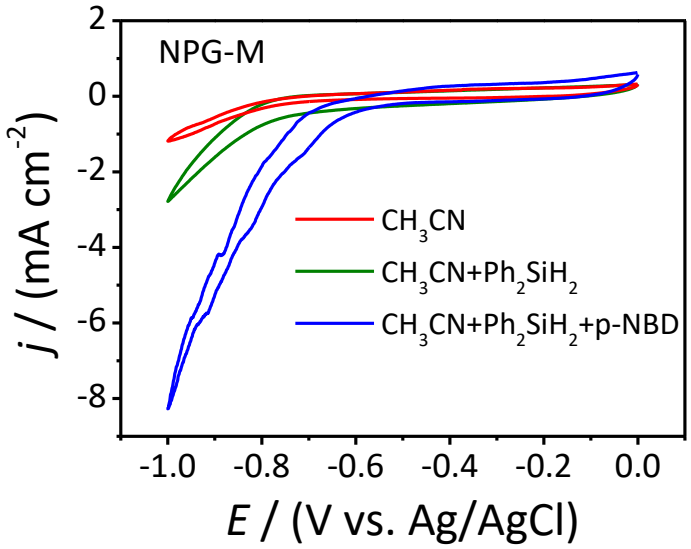

Fig. S6 CV curves of the NPG-M electrode in CH_3CN with or without substrates. Substrates: 1 mmol *p*-NBD, 1 mmol Ph_2SiH_2.

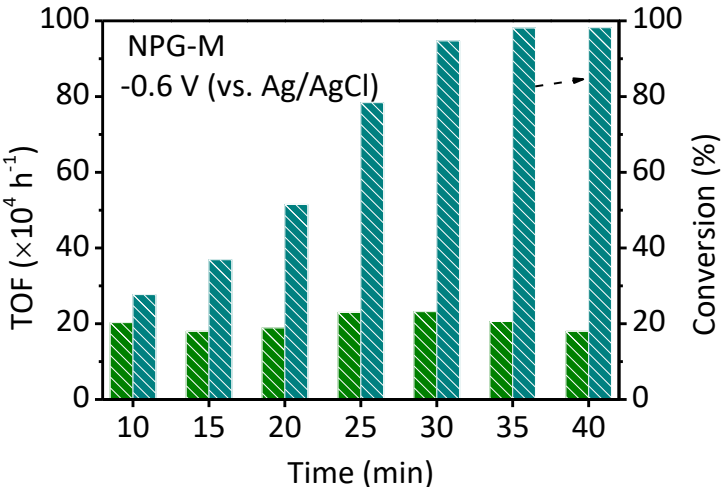

Fig. S7 Electrochemical catalytic performance of NPG-M as a function of reaction time at a potential of -0.6 V (vs. Ag/AgCl).

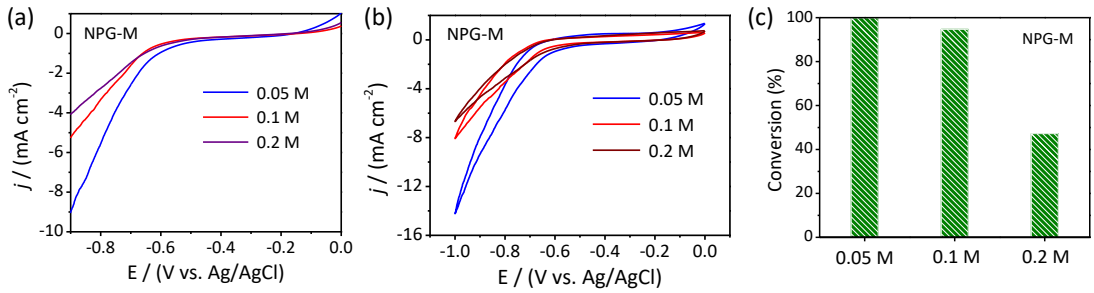

Fig. S8 LSVs (a) and CVs (b) of the NPG-M electrode in *p*-NBD/CH_3CN solution with different concentration; Influence of *p*-NBD concentration on catalytic performance of the NPG-M electrode.

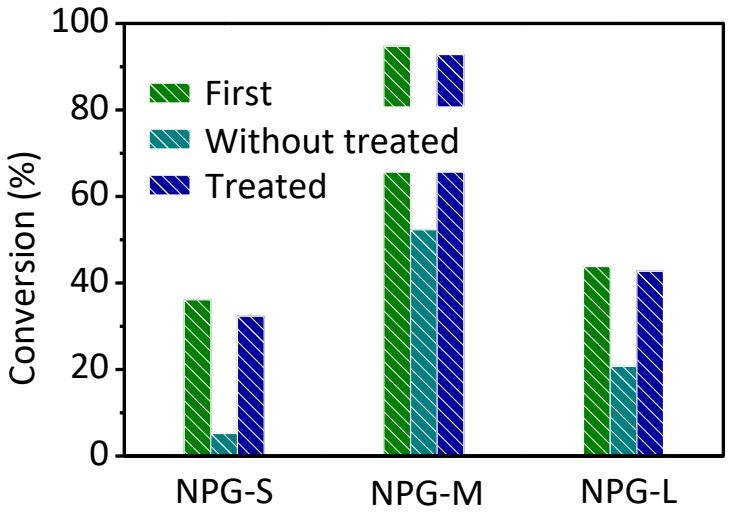

Fig. S9 Comparison of catalytic performance of NPG catalysts with or without activation treatment (activated at -0.8 V for 5 min in CH_3CN).

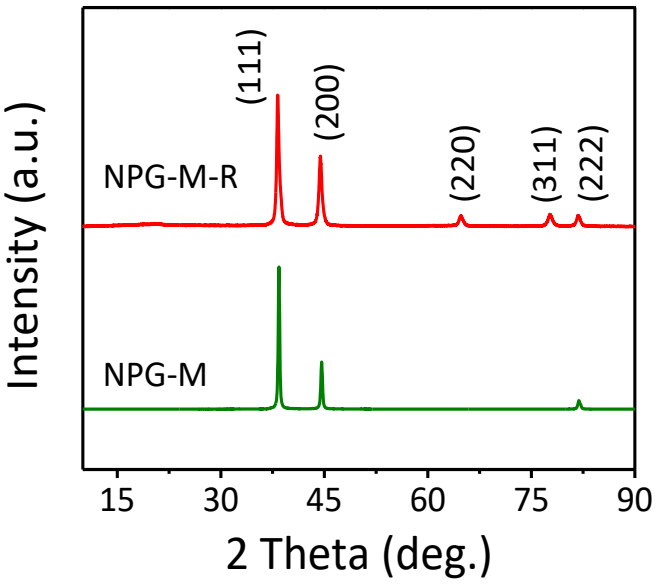

Fig. S10 XRD patterns for the NPG-M before and after reaction.

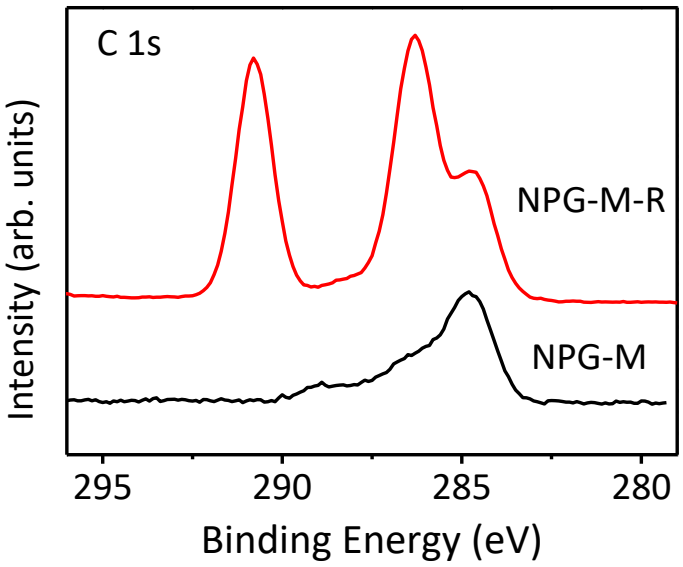

Fig. S11 C 1s spectra for the NPG before and after reaction.

Table S1 Comparison of catalytic performance on selective reduction of *p*-NBD for the NPG and literature reported catalysts.

Catalysts	Conditions	Conversion	Selectivity	TOF (h^{-1})	Ref.
Ru complexes	50 bar of H_2, 80 °C, 12 h	100%	100%	162.5	[1]
Iron(II) complexes	$PhSiH_3$, 60 °C, 1 h	100%	100%	200	[2]
Ni(II) complexes	$NaBH_4$, rt, 2 h	99%	100%	500	[3]
Iridium clusters	H_2, 30 °C, 1 h	98%	83%	40.7	[4]
$Au_n(SG)_m$	20 bar of H_2, 80 °C, 9 h	83.2%	100%	46.2	[5]
$Au_{99}(SPh)_{42}$	20 bar of H_2, 80 °C, 12 h	93.1%	100%	93.7	[6]
Au nanorod	20 bar of H_2, 80 °C, 8h, pyridine	53.2%	100%	2.6	[7]
$Au_{25}(SPh)_{18}$	20 bar of H_2, 80 °C, 10 h, pyridine	97%	100%	33.7	[8]
$Au_{38}(SR)_{24}$	HCOOK, 80 °C, 12 h	91%	100%	41.4	[9]
Au/Al_2O_3	H_2, 170 °C	-	100%	-	[10]
NPG-S	Ph_2SiH_2, rt, 0.5 h	36.1%	100%	1185 (4.6×10^4)	This work
NPG-M	Ph_2SiH_2, rt, 0.5 h	94.7%	100%	3109 (23.2×10^4)	This work
NPG-L	Ph_2SiH_2, rt, 0.5 h	43.8%	100%	1438 (14.9×10^4)	This work

Analytical Data

(4-nitrophenyl)methanol (2a) [11]

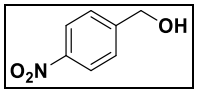

99% yield. ^{1}H NMR (400 MHz, $CDCl_3$) δ 8.20 (d, *J* =8,2 Hz, 2 H), 7.53 (d, *J* =8.2 Hz, 2 H), 4.83 (s, 2 H), 2.39 (bs, 1 H).

(2-nitrophenyl)methanol (2b) [12]

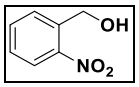

98% yield. ^{1}H NMR (400 MHz, $CDCl_3$) δ 8.11 (d, *J* =8.1 Hz, 1 H), 7.75 (d, *J* =7.7 Hz, 1 H), 7.68 (t, *J* =7.5 Hz, 1 H), 7.48 (t, *J* =7.8 Hz, 1 H), 4.98 (s, 2 H), 2.60 (br s, 1 H).

(3-nitrophenyl)methanol (2c) [13]

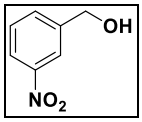

95% yield. ^{1}H NMR (400 MHz, $CDCl_3$) δ =8.24 (s, 1 H), 8.14 (d, *J* =8.4 Hz, 1 H), 7.70 (d, *J* =7.6 Hz, 1 H), 7.53 (t, *J* =8.0 Hz, 1 H), 4.82 (s, 2 H).

(4-(methylsulfonyl)phenyl)methanol (2d) [11]

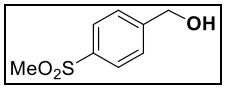

93% yield. ^{1}H NMR (400 MHz, $CDCl_3$) δ 7.78 (d, *J* =8.2Hz, 2 H), 7.48 (d, *J* =8.2Hz, 2 H), 4.74 (s, 2 H), 3.12 (s, 1 H), 3.01 (s, 3 H).

(4-(trifluoromethyl)phenyl)methanol (2e) [14]

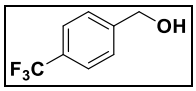

99% yield. ^{1}H NMR (400 MHz, $CDCl_3$) δ 7.56 (d, *J* =8.1 Hz, 2 H), 7.40 (d, *J* =8.1 Hz, 2 H), 4.65 (d, *J* =4.0 Hz, 2 H), 4.00 (s, 1 H).

4-(hydroxymethyl)benzaldehyde (2f) [15]

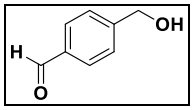

91% yield. ^{1}H NMR (400 MHz, $CDCl_3$) δ 9.96 (s, 1 H), 7.83 (d, *J* =8.0 Hz, 2 H), 7.50 (d, *J* =8.0 Hz, 2 H), 4.77 (s, 2 H).

(4-ethynylphenyl)methanol (2g) [16]

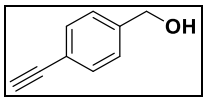

96% yield. ^{1}H NMR (400 MHz, $CDCl_3$) δ 7.49 (d, *J* =8.1 Hz, 2 H), 7.32 (d, *J* =8.1 Hz, 2 H), 4.70 (d, *J* =5.6 Hz, 2 H), 3.07 (s, 1 H), 1.71 (t, *J* =5.6 Hz, 1 H).

4-(hydroxymethyl)benzonitrile (2h) [14]

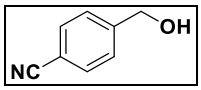

99% yield. ^{1}H NMR (400 MHz, $CDCl_3$): δ 7.64-7.60 (m, 2H), 7.47-7.44 (m, 2H), 4.76 (s, 2H), 2.16 (bs, 1H).

[1,1'-biphenyl]-4-ylmethanol (2i) [17]

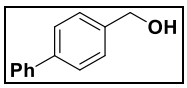

99% yield. ^{1}H NMR (400 MHz, $CDCl_3$): δ 7.63–7.59 (m, 4 H), 7.48–7.43 (m, 4 H), 7.40–7.36 (m, 1 H), 4.73 (s, 2 H), 2.08 (bs, 1 H).

Pyridin-2-ylmethanol (2j) [15]

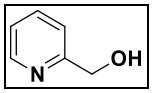

99% yield. ^{1}H NMR (400 MHz, $CDCl_3$) δ 8.45 (s, 1 H), 8.38 (d, *J* =3.8 Hz, 1 H), 7.69 (d, *J* =7.5 Hz, 2 H), 7.24 (t, *J* =6.1 Hz, 1 H), 4.66 (s, 2 H).

quinolin-4-ylmethanol(2k) [18]

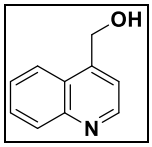

94% yield. ^{1}H NMR 400 MHz, $CDCl_3$) δ 8.87 (d, *J* =4.4 Hz, 1 H), 8.11-8.16 (m, 1H), 7.93-7.98 (m, 1H), 7.68-7.76 (m, 1H), 7.52-7.61 (m, 2H), 5.23 (d, *J* =4.2 Hz, 2H).

(E)-3-(furan-2-yl)prop-2-en-1-ol (2j) [13]

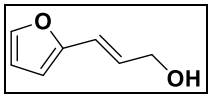

96% yield. ^{1}H NMR (400 MHz, $CDCl_3$) δ 7.33 (d, *J* =1.6 Hz, 1 H), 6.42 (dt, *J* =15.6, 1.6 Hz, 1 H), 6.35 (dd, *J* =3.2, 1.6 Hz, 1 H), 6.27 (dt, *J* =16.0, 5.6 Hz, 1 H), 6.22 (d, *J* =3.2 Hz, 1 H), 4.27 (dd, *J* =5.6, 1.6 Hz, 2 H).

(E)-3-phenylprop-2-en-1-ol (2k) [14]

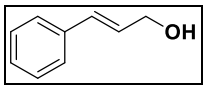

86% yield. ^{1}H NMR (400 MHz, $CDCl_3$) δ 7.34 (d, *J* =8.0 Hz, 2 H), 7.28 (t, *J* =8.0 Hz, 2 H), 7.20-7.23 (m,1 H), 6.56 (d, *J* =12.1 Hz, 1 H), 6.28-6.34 (m, 1 H), 4.26 (d, *J* =4.2 Hz, 2 H), 3.10 (bs, 1 H).

3-(benzo[d][1,3]dioxol-5-yl)-2-methylpropan-1-ol (2l) [19]

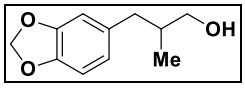

92% yield. ^{1}H NMR (250 MHz, $CDCl_3$) δ 6.82–6.57 (m, 3 H), 5.94 (s, 2 H), 3.60–3.42 (m, 2 H), 2.69 (dd, *J* =13.5, 6.3 Hz, 1 H), 2.37 (dd, *J* =13.5, 8.0 Hz, 1 H), 1.90 (dq, *J* =13.1, 6.5 Hz, 1 H), 1.77 (s, 1 H), 0.93 (d, *J*=6.7 Hz, 3 H).

1-(thiophen-3-yl)ethan-1-ol (2m) [20]

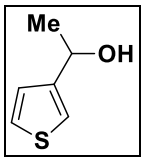

90% yield. ^{1}H NMR (400 MHz, $CDCl_3$) δ 1.60 (d, *J* =6.4 Hz, 3 H), 5.12 (q, *J* =6.4 Hz, 1 H), 6.96 (d, *J* =8.0 Hz, 2 H), 7.22-7.24 (m, 1 H).

1-(4-nitrophenyl)ethan-1-ol (2n) [13]

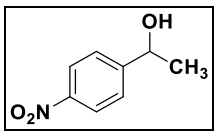

95% yield. ^{1}H NMR (400 MHz, $CDCl_3$) δ 8.20 (d, *J* =8.8 Hz, 2 H), 7.54 (d, *J* =8.8 Hz, 2 H), 5.05-4.99 (m, 1 H), 1.51 (d, *J* = 5.6 Hz, 3 H).

(4-nitrophenyl)(phenyl)methanol (2p) [21]

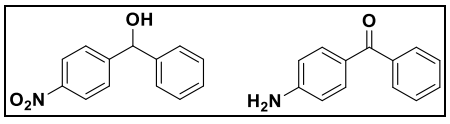

95% yield (3% nitro reduction product was detected). ^{1}H NMR (400 MHz, $CDCl_3$) δ 8.19–8.16 (m, 2 H), 7.58–7.55 (m, 2 H), 7.40–7.30 (m, 5 H), 5.91 (d, *J* =2.8 Hz, 1 H), 2.47 (d, *J* =2.8 Hz, 1 H)

References

1 A. Indra, N. Maity, P. Maity, S. Bhaduri and G. K. Lahiri, *J. Catal.*, 2011, **284**, 176–183.

2 C. Johnson and M. Albrecht, *Organometallics*, 2017, **36**, 2902–2913.

3 Y. Jiang, M. Li, X. Liang, J. Mack, M. Wildervanck, T. Nyokong, M. Qin and W. Zhu, *Dalt. Trans.*, 2015, **44**, 18237–18246.

4 T. Higaki, H. Kitazawa, S. Yamazoe and T. Tsukuda, *Nanoscale*, 2016, **8**, 11371–11374.

5 G. Li, D. E. Jiang, S. Kumar, Y. Chen and R. Jin, *ACS Catal.*, 2014, **4**, 2463–2469.

6 G. Li, C. Zeng and R. Jin, *J. Am. Chem. Soc.*, 2014, **136**, 3673–3679.

7 G. Li, C. Zeng and R. Jin, *J. Phys. Chem. C*, 2015, **119**, 11143–11147.

8 C. Liu, H. Abroshan, C. Yan, G. Li and M. Haruta, *ACS Catal.*, 2016, **6**, 92–99.

9 J. Zhao, Q. Li, S. Zhuang, Y. Song, D. J. Morris, M. Zhou, Z. Wu, P. Zhang and R. Jin, *J. Phys. Chem. Lett.*, 2018, **9**, 7173–7179.

10 N. Perret, X. Wang, T. Onfroy, C. Calers and M. A. Keane, *J. Catal.*, 2014, **309**, 333–342.

11 M. Gavel, T. Courant, A. Y. P. Joosten and T. Lecourt, *Org. Lett.*, 2019, **21**, 1948–1952.

12 R. Wang, Y. Tang, M. Xu, C. Meng and F. Li, *J. Org. Chem.*, 2018, **83**, 2274–2281.

13 J. Wei, L. Zhao, C. He, S. Zheng, J. N. H. Reek and C. Duan, *J. Am. Chem. Soc.*, 2019, **141**, 12707–12716.

14 S. R. Tamang, D. Bedi, S. Shafiei-Haghighi, C. R. Smith, C. Crawford and M. Findlater, *Org. Lett.*, 2018, **20**, 6695–6700.

15 S. Sharma, D. Bhattacherjee and P. Das, *Adv. Synth. Catal.*, 2018, **360**, 2131–2137.

16 J. Ando, M. Asanuma, K. Dodo, H. Yamakoshi, S. Kawata, K. Fujita and M. Sodeoka, *J. Am. Chem. Soc.*, 2016, **138**, 13901–13910.

17 D. Wei, A. Bruneau-Voisine, T. Chauvin, V. Dorcet, T. Roisnel, D. A. Valyaev, N. Lugan and J.-B. Sortais, *Adv. Synth. Catal.*, 2018, **360**, 676–681.

18 M. Mikołajczyk, J. A. Krysiak, W. H. Midura, M. W. Wieczorek and E. Różycka-Sokołowska, *J. Org. Chem.*, 2006, **71**, 8818–8823.

19 S. Weber, J. Brünig, V. Zeindlhofer, C. Schröder, B. Stöger, A. Limbeck, K. Kirchner and K. Bica, *ChemCatChem*, 2018, **10**, 4386–4394.

20 S. Ganesamoorthy, P. Jerome, K. Shanmugasundaram and R. Karvembu, *RSC Adv.*, 2014, **4**, 27955–27962.

21 T. Touge, H. Nara, M. Fujiwhara, Y. Kayaki and T. Ikariya, *J. Am. Chem. Soc.*, 2016, **138**, 10084–10087.